

ORIGINAL RESEARCH

Open Access



Novel chaos game optimization tuned-fractional-order PID fractional-order PI controller for load-frequency control of interconnected power systems

Mohamed Barakat*

Abstract

In this work, chaos game optimization (CGO), a robust optimization approach, is employed for efficient design of a novel cascade controller for four test systems with interconnected power systems (IPSs) to tackle load-frequency control (LFC) difficulties. The CGO method is based on chaos theory principles, in which the structure of fractals is seen via the chaotic game principle and the fractals' self-similarity characteristics are considered. CGO is applied in LFC studies as a novel application, which reveals further research gaps to be filled. For practical implementation, it is also highly desirable to keep the controller structure simple. Accordingly, in this paper, a CGO-based controller of fractional-order (FO) proportional–integral–derivative–FO proportional–integral (FOPID–FOPI) controller is proposed, and the integral time multiplied absolute error performance function is used. Initially, the proposed CGO-based FOPID–FOPI controller is tested with and without the nonlinearity of the governor dead band for a two-area two-source model of a non-reheat unit. This is a common test system in the literature. A two-area multi-unit system with reheater–hydro–gas in both areas is implemented. To further generalize the advantages of the proposed scheme, a model of a three-area hydrothermal IPS including generation rate constraint nonlinearity is employed. For each test system, comparisons with relevant existing studies are performed. These demonstrate the superiority of the proposed scheme in reducing settling time, and frequency and tie-line power deviations.

Keywords: Interconnected power system, Chaos game optimization, Cascade control, Load frequency control, FOPID–FOPI controller, Generation rate constraint (GRC), Governor dead band (GDB)

1 Introduction

In power systems, power generation needs to meet customer demand. As a result, the system must remain stable under high step-load perturbations (SLPs) to regulate frequency instability. The main part of automatic generation control (AGC) is load–frequency control (LFC), which is required for maintaining nominal tie-line power and nominal system frequency during disturbances. The regulated output of the AGC is an area control error

(ACE), which is guided to zero to eliminate frequency and tie-line power deviations [1, 2]. The following summarizes an LFC's primary responsibilities [3]:

- At steady state, each region should be able to support its own load.
- During the transition period, areas in need of electricity might partner with one another.
- The system must be kept under control during an abrupt load interruption and any other disruptions.
- The frequency and tie-line power deviations in terms of overshoot, undershoot, and settling time should be minimized to enhance system stability.

*Correspondence: mhabbarakat@yahoo.com
Communication and Computer Department, Faculty of Engineering,
Nahda University, Bani-Sweif, Egypt

As a result, various LFC controlling methods have been established to maintain tie-line power and system frequency with minimum changes, such as proportional–integral (PI) [4], integral–derivative (ID) [5], proportional–integral–derivative (PID) [6], and optimal PID [7] controllers. To achieve better performance, LFC is built using a fuzzy scheme in [8], and an adaptive fuzzy scheme for a PI scheme is described in [9]. These approaches are difficult to execute, and success cannot be guaranteed. Recently, soft computing schemes for addressing LFC issues in an interconnected power system (IPS) have been designed. LFC research focusing on the design of classical integer controllers has been extensive, e.g., bacterial-foraging optimization (BFO)-based PID [10], differential-evolution (DE)-based PID [11], teaching–learning-based optimization (TLBO)-based PID [12], and 2DOF-PID [13]. Nonlinear LFC problems and system stability under large SLPs and uncertainties have been addressed using novel control techniques, such as the adaptive neuro fuzzy inference system (ANFIS) [14], model predictive control [15, 16], fuzzy logic [17, 18], and artificial neural networks [19]. For integration of renewable energy, such as wind energy, a grouped grey wolf optimizer based interactive PI controller for maximum power point tracking and democratic joint operations algorithm based PID controller for optimum power extraction are presented in [20, 21], respectively.

Because of the growing complexity of IPSs, such as high load disruptions and nonlinearities, the performance of non-CCs deteriorates significantly [22]. In the case of non-CCs, there are fewer tuning parameters than with CCs. However, with more tuning parameters in the controller structure, it can produce better results. Hence, the CC structure is one of the most effective controller techniques for improving the performance of a control system, especially with disturbances and parameter uncertainties [23–25]. Consequently, CCs for AGC, such as the Bat algorithm-based PD-PID CC [26], modified gray wolf optimizer (MGWO)-based PI-PD and CC-TID, are presented in [27, 28], respectively, simplified GWO (SGWO)-based adaptive fuzzy PID controller is given in [29], and a maiden application of the slap swarm algorithm-based TID-TID CC is presented in [22].

An AGC control strategy must be able to deal effectively with nonlinearities such as governor dead band (GDB) and generation rate constraint (GRC), parameter uncertainties, and disturbances while still achieving the desired dynamic performance. In addition, the controller application should not be overly complex in order to provide a realistic solution for engineering problems. Recently, FO calculus has also been used. These controllers are computationally more powerful in enhancing the performance than conventional

methods because they remove the limitations produced by their traditional counterparts, and it has been confirmed that they can achieve significant efficiency improvements [23, 30, 31]. A Yin-Yang-Pair optimization-based FOPID controller is presented in [32] to harvest the maximum solar power from the PV arrays, while control of superconducting magnetic energy storage systems in grid-connected microgrids using the slap swarm algorithm based-FOPID is proposed in [33]. The adaptive FO-fuzzy-PID controller optimized by the TLBO algorithm is presented, where all the controller parameters are tuned simultaneously to handle the uncertainties caused by renewable sources, parametric and load variations [34]. An LFC strategy via FO controllers is introduced and compared with classical ones to demonstrate the superiority of FO, where the fraction of integral and derivative parts lie within the [0, 1] range [30, 35–38]. A recent innovation in this method is where the fractional integral and derivative parts do not necessarily lie within the [0, 1] range, but can be any real numbers for the differentiator and integrator orders that exhibit better dynamic response with excellent robustness to parameter uncertainties and external disturbances [23, 39–41].

Finally, to attain the best performance, a powerful optimizer must be applied [42, 43]. Therefore, a new and powerful algorithm such as the chaos game optimizer (CGO) is used [44]. The main idea of the CGO technique is based on the principles of chaos theory, wherein the structure of fractals by the chaos game principle and the fractal problems of self-similarity are considered. CGO has some advantages over other swarm schemes, such as fast convergence and avoiding trapping in a local minimum [44]. Thus, CGO has been used in solving many engineering problems [45–47]. From the above discussion, the controller enhancements come from the appropriate fractional calculus, using a cascade controller (CC), and fine-tuning of CC parameters using a powerful optimizer. Therefore, in this paper, a combination of CGO and a novel cascade FOPID–FOPI controller is proposed. This combination (CGO: FOPID–FOPI) is employed based on an integral of time multiplied by the absolute error (ITAE) criterion as a secondary controller for the study of LFC in four test systems, to demonstrate the effectiveness and robustness of the proposed CGO: FOPID–FOPI scheme.

In summary, the main contributions of this study are as follows:

1. The deployment of the novel CGO-based controller for dealing with LFC problems.
2. Optimization of the FOPID–FOPI controller parameters using four different IPS test systems.

3. Dynamic analysis in the presence of nonlinearities, which demonstrates the superior performance of CGO: FOPID–FOPI.
4. Comparison of the dynamic performance of the CGO: FOPID–FOPI controller with those of recently developed soft-computing-based controllers.

2 Systems study

2.1 Two-area IPS for a thermal unit (Test-systems 1, 2)

First, investigations are conducted on a two-area IPS with and without GDB nonlinearity. The parameters of the two systems are presented in “Appendices 1 and 2”, respectively.

The two systems are referred to as Test-system 1 (without GDB) and Test-system 2 (with GDB) as shown in Fig. 1. Their transfer function (TF) models are frequently used in the literature as common test systems [10, 13, 23, 48, 49]. Each non-reheat power plant consists of a speed governing system, turbine, and generator, and has three inputs and two outputs [13]. The inputs are the tie-line power deviation ΔP_{tie} , controller output ΔP_{ref} and the SLP (ΔP_L), and the outputs are the generator frequency deviation Δf , and the ACE calculated as [13]:

$$\text{ACE} = B\Delta f \pm \Delta P_{tie}, \quad (1)$$

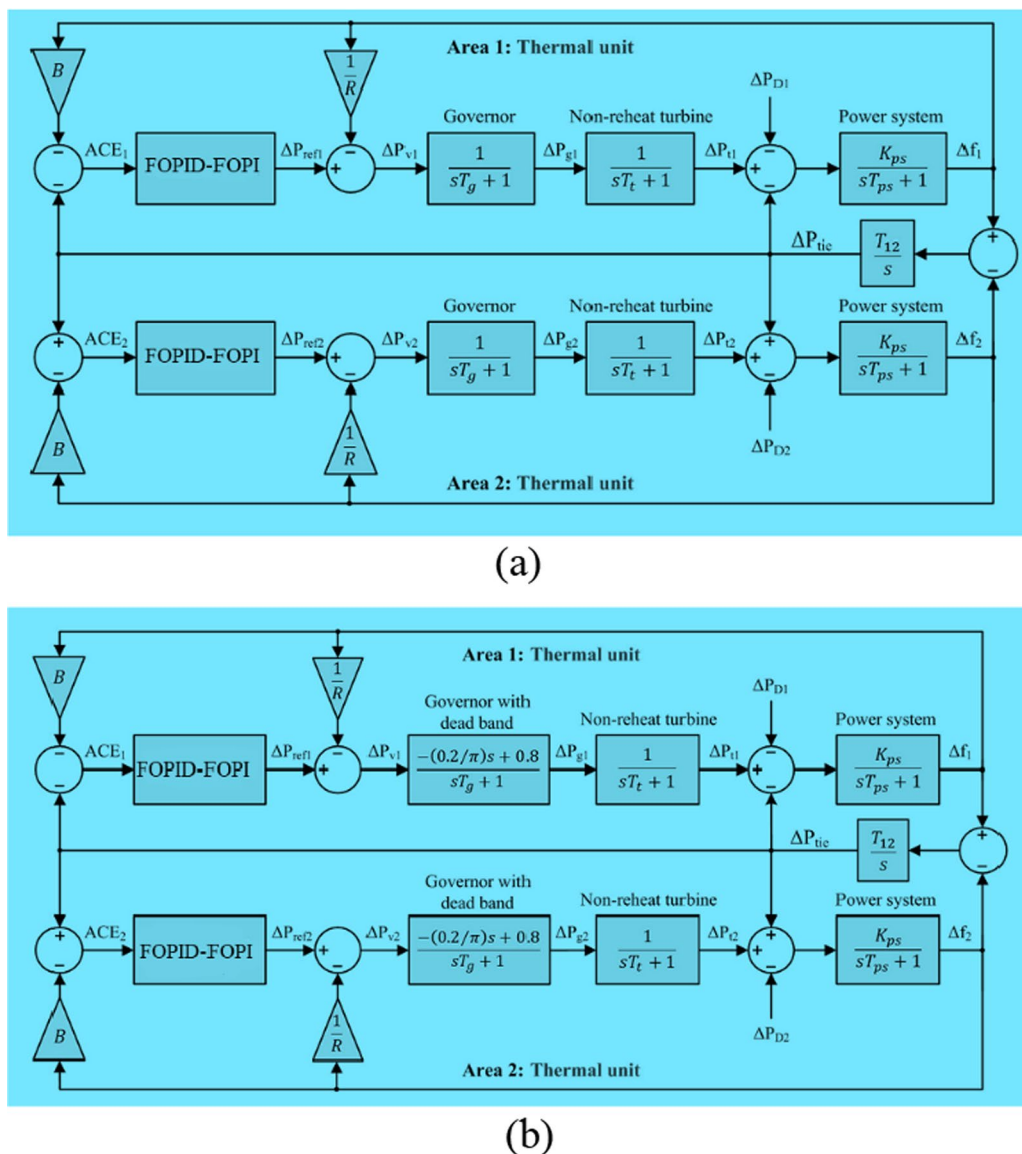


Fig. 1 TF model of the two-area nonthermal unit: **a** without GDB (Test-system 1) and **b** with GDB (Test-system 2)

where B is the frequency bias parameter. The TFs are used to designate each component in the system [13]. For non-reheat turbines, the TF is simple because it is exhibited as a first-order TF with a time constant T_t , as:

$$G_T(s) = \frac{1}{1 + T_t S}, \quad (2)$$

When the load changes, the frequency fluctuates. The control system detects these fluctuations and adjusts the turbine to dampen the frequency fluctuations. The governor TF is modeled as:

$$G_G(s) = \frac{1}{1 + T_g S} \quad (3)$$

Because the response of the governor valve to the fluctuation of the small input signal is inapplicable, the nonlinearity of GDB is considered. The nonlinearity of GDB causes more fluctuations and degrades the overall stability of the power system [48]. The governor TF with GDB is modeled as:

$$C_g = \frac{0.8 - \frac{0.2}{\pi} S}{1 + T_g S} \quad (4)$$

The governor system has two inputs ΔP_{ref} and Δf , and provides an output ΔP_G , which is presented by [13]:

$$\Delta P_G = \Delta P_{ref} - \frac{1}{R} \Delta f, \quad (5)$$

where R is the speed regulation parameter. The general TF of the generator-load is described by:

$$G_P(s) = \frac{K_{PS}}{1 + T_{PS} S} \quad (6)$$

where K_{PS} and T_{PS} are the power system gain and time constant, respectively [13, 48]. Because of the similarity of both areas in Test-systems 1 and 2, similar controllers with the same gains are employed in areas 1 and 2.

2.2 Two-area multisource power system (Test-system 3)

To further characterize the performance of the CGO-tuned FOPID-FOPI CC, the study is expanded to a more practical multi-source IPS. The two-area six-unit IPS consists of more power generating sources such as reheat, hydro, and gas units in both area 1 and area 2 with a rating of 2000 MW, and the load is 1840 MW [10, 11, 13]. The two-area six-unit system is broadly applied and is used for the design and analysis of the automatic LFC for IPS, and its TF is displayed in Fig. 2. The nominal parameters of the studied system are displayed in "Appendix 3". The load change ΔP_L is mimicked to be close to an actual load using [50]:

$$\Delta P_L = 0.6 \sqrt{P_{Load}} \quad (7)$$

Therefore, $\Delta P_L = 25$ MW, which is 1.25% SLP from the power rating. In this study, the investigations are done under 2% SLP to ensure the stability of the proposed controller. Because the two areas are equivalent, the three controllers in both areas are the same. This avoids the requirement for tuning of the six controllers for the six units, which would be costly in terms of optimizing and impractical for operation.

2.3 Three-area hydrothermal IPS (Test-system 4)

A three-area thermal–thermal–hydro IPS is established and used to test the proposed approach's capability of coping with a multi-area multi-source IPS. This system, called Test-system 4, is shown in Fig. 3, and the system parameters are listed in "Appendix 4". It is generally recognized that power generation cannot change at an unlimited rate because of the system physics and dynamics. To limit the rate of generation change, a substantial limitation known as GRC is considered for all the areas in Fig. 3. The benchmark value of GRC for thermal plants according to the literature is 3% per min [23]. For the third area (hydro), a GRC of 360% per minute for decreasing generation and 270% per minute for increasing generation, are considered. In Test-systems 3 and 4, three controllers with several parameters must be adjusted at the same time. As a result, a strong optimizer such as CGO is required to achieve the desired performance.

3 Control-approach-based performance function

3.1 Fractional-order controller

Because of their quick reaction time, strong stability under varied conditions, and excellent resilience to perturbations, fractional-order (FO) controllers have seen a notable increase in use in control system engineering. As a result, research using the FOPID controller has been conducted in a variety of application fields such as speed control of DC motors [37, 51], heat flow processes [52], and autonomous microgrid VSC systems [31], as well as LFC of IPS as previously mentioned. A common FO controller based on FO calculus is FOPIID, which is referred to as $PI^\lambda D^\mu$ where λ and μ are the integral and derivative parts of non-integer orders. The TF of the FOPID controller is:

$$G_{FOPID}(s) = K_p + \frac{K_I}{S^\lambda} + K_D s^\mu, \quad (8)$$

The enhancement of performance comes from the fine-tuning of the integral and derivative parts (λ and μ) besides the proportional (K_p), integral (K_I), and derivative (K_D) gains. The tuning of λ and μ produces many

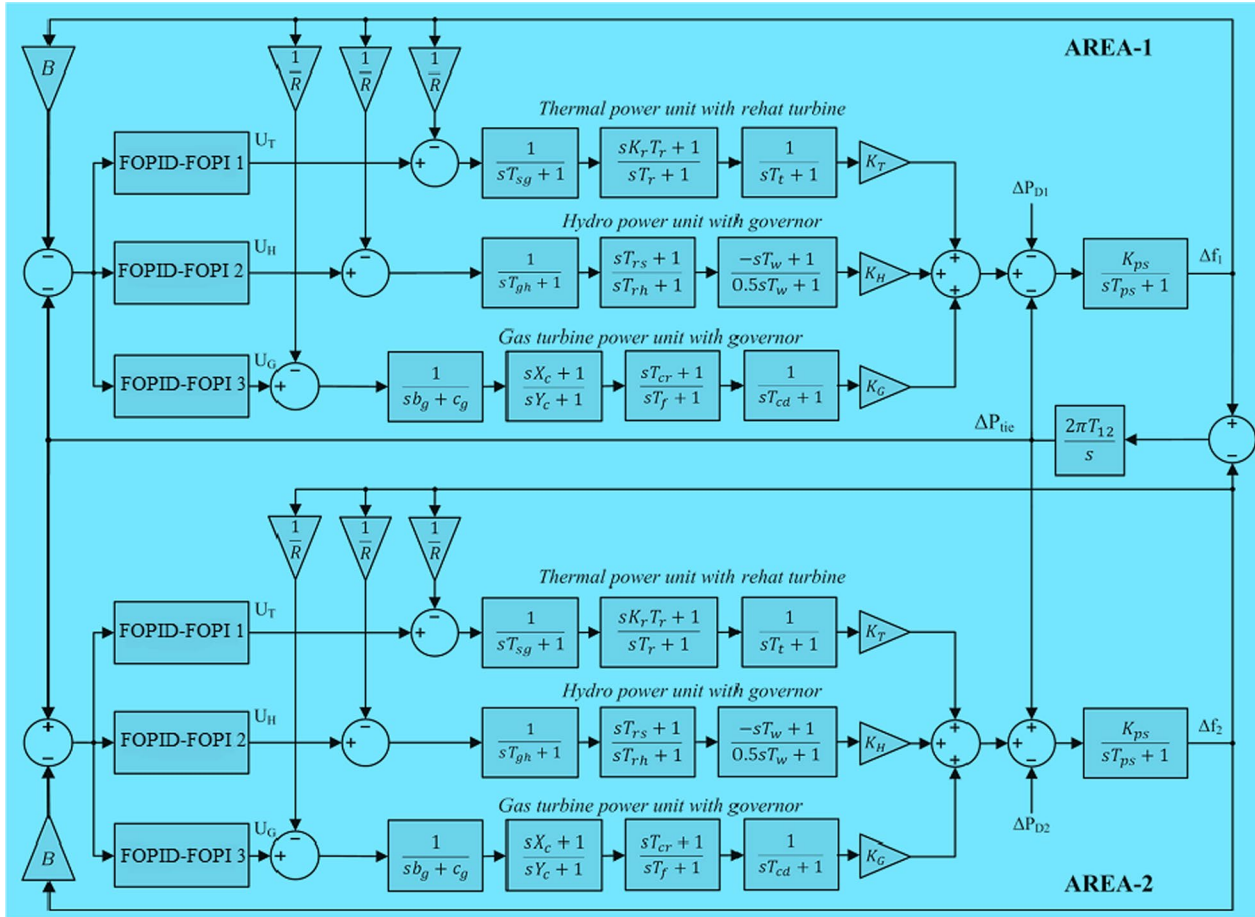


Fig. 2 TF model of two-area multi-source system (Test-system 3)

controller structures. In real-time applications and computer simulations, the fraction TF of s is required to approximate to an integer-order TF. The Oustaloup filter offers this approximation within a frequency band $[\omega_L, \omega_H]$, where ω_L is the lower frequency and ω_H is the higher frequency with order N as follows [53]:

$$G_f(s) = S^\alpha = K \prod_{k=-N}^N \frac{s + \omega_k^z}{s + \omega_k^p}, \quad (9)$$

where K is the gain of the filter, ω_k^p and ω_k^z are the poles and zeroes of $G_f(s)$, respectively.

From (9), two critical factors can significantly impact the performance of the approximation, i.e., the approximation order N , and filter gain K . K is adjusted so that the approximate gain is unity at 1 rad/s. Lower N values result in easier approximation and simpler implementation, but efficiency degrades because of ripple development in the phase and magnitude response. Increasing the N value complicates the approximation and makes computation hard in real-time implementation.

Therefore, choosing N is a trade-off between complexity and accuracy. In this study, $N=5$ and a fitting frequency band within $[10^{-3} : 10^3]$ rad/s is considered.

3.2 Proposed FOPID–FOPI CC

This study proposes a FOPID–FOPI CC to improve LFC performance in four IPS test systems. Figure 4a shows the proposed FOPID–FOPI CC scheme, which has not been used previously in LFC research. The processing time in any optimization problem directly depends on the number of variables in the problem. Therefore, in simulation mode, to reduce the number of controller variables, the fraction integral $\lambda 1$ and the fraction derivative μ are set within the $[0, 1.5]$ range. To reduce the complexity in real implementation, instead of $\lambda 1$ and μ , two cascaded fraction integrals $\lambda 11$ and $\lambda 12$ and two cascaded fraction derivatives $\mu 11$ and $\mu 12$ for the first FOPID controller are designed, respectively. The range of $\lambda 11$, $\mu 11$, and $\lambda 21$ lie within $[0, 1]$ range, while $\lambda 12$ and $\mu 12$ lie within $[0, 0.5]$ range as shown in Fig. 4b. For example: (i) if $\lambda 1 \geq 1$, it sets $\lambda 11 = 1$ and $\lambda 12$ equals the fraction that is more than 1;

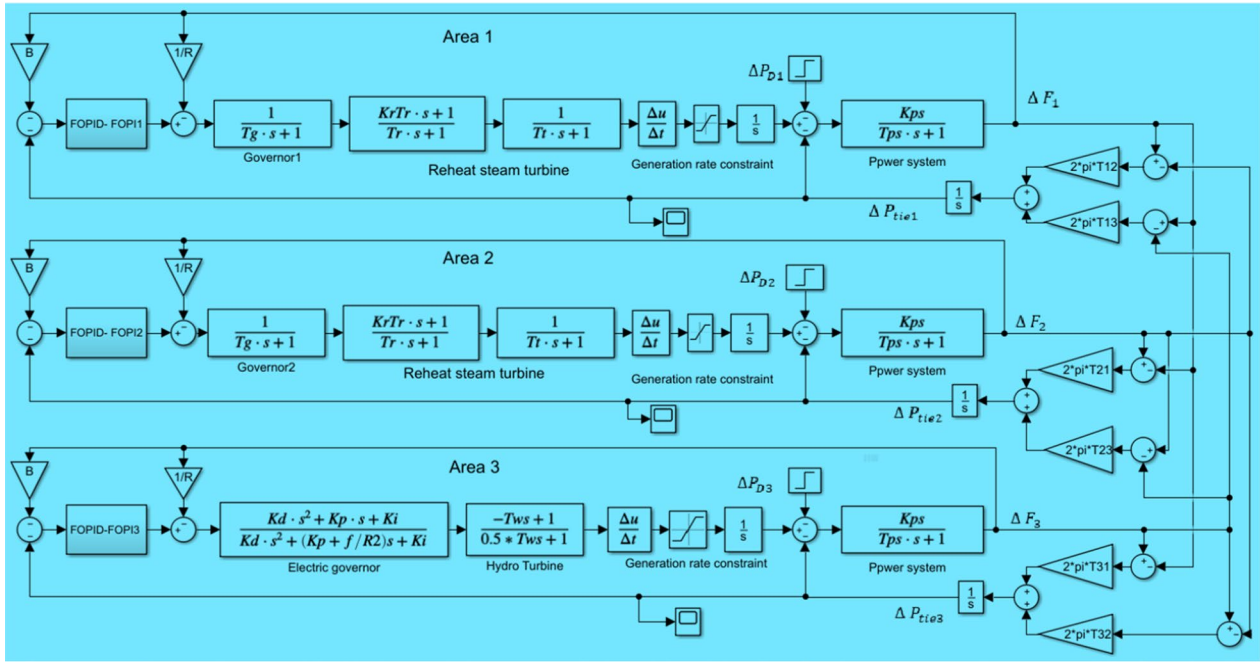


Fig. 3 TF model of three-area multi-source IPS (Test-system 4)

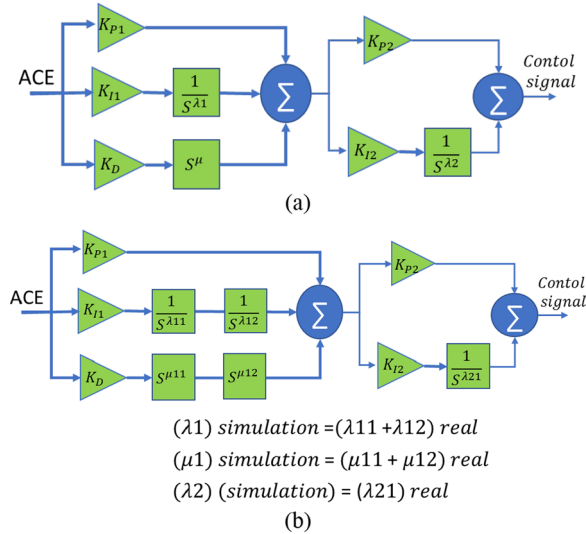


Fig. 4 a Proposed FOPID-FOPI controller structure reduced variables (simulation mode), b proposed FOPID-FOPI controller structure (for real implementation)

(ii) If $\lambda_{11} < 1$, λ_{11} equals the fraction that is less than 1 and $\lambda_{12} = 0$. These settings are also applied at μ . The main objectives of CC are for the internal process (FOPID)

to attenuate the effect of a supply disruption while the external process (FOPI) manages the final production quality [54]. A CC system can be used to quickly reject a disturbance, before it spreads to other parts of the system, to attain greater performance [26]. To implement the FOPID–FOPI CC system for the investigated process, a powerful new CGO scheme is demonstrated.

3.3 Optimization of the FOPID–FOPI CC

In power systems, LFC must achieve two objectives under load perturbations, i.e., a return of the steady-state frequency to zero and maintenance of the power transfer at predetermined values. Therefore, the LFC should be tuned carefully by choosing the most suitable objective function, e.g., integral of absolute error, integral of time multiplied by squared error, integral of squared error, and ITAE. ITAE is the most meaningful objective in LFC design [11, 12]. The optimization is confirmed by reducing the value of the objective function given by the ITAE as follows:

$$J_{ITAE} \text{ (Two areas)}$$

$$= \int_0^{t_{sim}} (|\Delta F_1| + |\Delta F_2| + |\Delta P_{tie12}|) \cdot t \cdot dt, \quad (10)$$

$$J_{ITAE} (\text{Three area}) = \int_0^{t_{sim}} (|\Delta F_1| + |\Delta F_2| + |\Delta F_3| + |\Delta P_{tie12}| + |\Delta P_{tie13}| + |\Delta P_{tie23}|).t.dt, \quad (11)$$

where t_{sim} is the simulation time. In this paper, the adopted optimization problem is defined as:

$$\text{Minimize } (ITAE) \quad (12)$$

which is subject to:

$$\begin{aligned} K_{P1}^{\min} &\leq K_{P1} \leq K_{P1}^{\max} \\ K_{P2}^{\min} &\leq K_{P2} \leq K_{P2}^{\max} \\ K_{I1}^{\min} &\leq K_{I1} \leq K_{I1}^{\max} \\ K_{I2}^{\min} &\leq K_{I2} \leq K_{I2}^{\max}, \\ K_D^{\min} &\leq K_D \leq K_D^{\max} \\ \lambda_1^{\min} &\leq \lambda_1 \leq \lambda_1^{\max} \\ \lambda_2^{\min} &\leq \lambda_2 \leq \lambda_2^{\max} \\ \mu^{\min} &\leq \mu \leq \mu^{\max} \end{aligned} \quad (13)$$

where \min and \max are the minimum and maximum gains of the employed FOPID–FOPI controller. The ranges of K_{P1} , K_{P2} , K_{I1} , K_{I2} , and K_D are within [0, 3] in Test-systems 1 and 2, and within [0, 2] in Test-systems 3 and 4, whereas the ranges of λ_1 and μ are within [0, 1.5] and [0, 1] for λ_2 in all test systems [23].

4 Chaos game optimization

The key idea of the CGO algorithm is based on certain concepts of chaos theory in which the structure of fractals by chaos game principles and the fractals' self-similarity problems are considered [44]. Design problems

have become extremely complex and traditional algorithms based on mathematical concepts are unable to produce satisfactory results. The implementation of an efficient new optimization algorithm is therefore of great interest if it can achieve high performance, high accuracy, and improved speed when dealing with complex problems. In the CGO algorithm, chaos game theory is used as the main algorithm concept, and the algorithm formula is based on game theory.

4.1 Inspiration

Chaos theory focuses on the randomness of complex processes that are sensitive to initial conditions, and applies to current key patterns, such as fractals, repeated templates, etc., [55]. Chaos theory reveals that small change in the system's initial conditions can result in very large changes in later conditions. In addition, the current state of the system can settle on the future state of the system, although the approximated current state can hardly determine the future state of the system.

Most chaos approaches include fractal graphical forms. A fractal is a geometric shape that is replicated in various scales and depicts them as self-similar structures. In mathematics, the chaos game is the method of constructing fractals using an initial polygon form with a random starting point. In this regard, the vertices of the main polygon/fractal should be arranged first, and an initial random point is chosen as the starting point

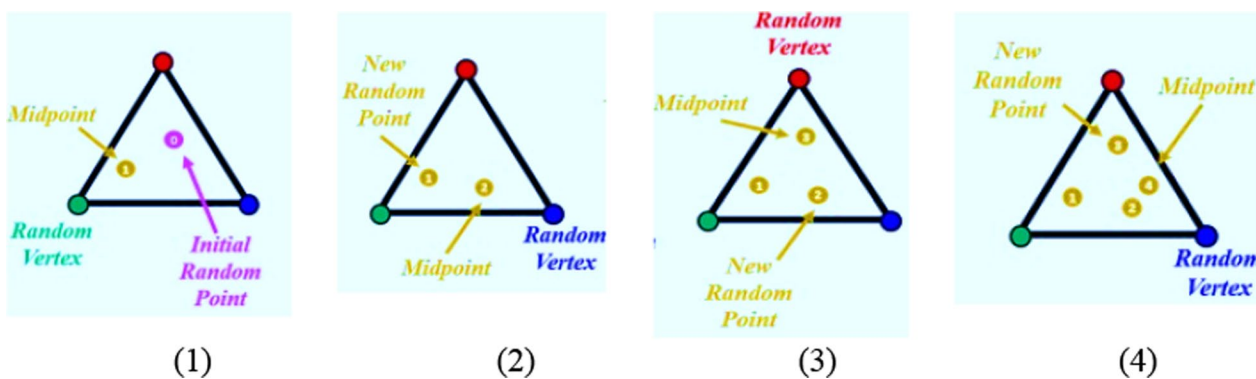


Fig. 5 Inspiration for CGO

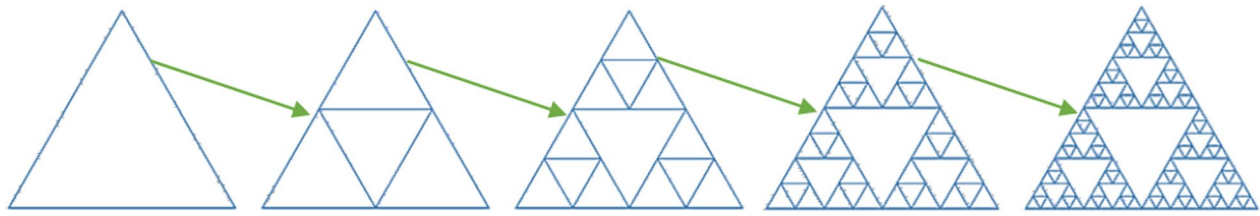


Fig. 6 Formation of the final shape and self-similarity of the Sierpinski triangle at different scales

for fractal construction. The next point is defined as a fraction of the distance between the initial point and one of the vertices of the polygon. The fractal is generated by repeating this process continuously, considering the random initial point and the random selection of the vertex in each iteration. The inspiration of CGO is shown in Fig. 5. The Sierpinski triangle is formed by using three vertices with a factor of 1/2. As the number of initial vertices for the fractal is increased to N , a Sierpinski with $N - 1$ dimensions can be created as presented in Fig. 6.

4.2 Mathematical model

Initially, the Sierpinski triangle is considered as the search space for solution candidates in the CGO algorithm. CGO considers several solutions (S), which denote some eligible seeds inside a Sierpinski triangle [56]. Each solution candidate (S_i) consists of some decision variables ($S_{i,j}$) which epitomize the position of the seeds as:

$$S = \begin{bmatrix} S_1 \\ S_2 \\ \vdots \\ S_i \\ \vdots \\ S_n \end{bmatrix} = \begin{bmatrix} s_1^1 & s_1^2 & \dots & s_1^j & \dots & s_1^d \\ s_2^1 & s_2^2 & \dots & s_2^j & \dots & s_2^d \\ \vdots & \vdots & \dots & \vdots & \dots & \vdots \\ s_i^1 & s_i^2 & \dots & s_i^j & \dots & s_i^d \\ \vdots & \vdots & \dots & \vdots & \dots & \vdots \\ s_n^1 & s_n^2 & \dots & s_n^j & \dots & s_n^d \end{bmatrix}, \quad (14)$$

$$\text{where } \begin{cases} i = 1, 2, \dots, n. \\ j = 1, 2, \dots, d. \end{cases}$$

where n is the number of solutions/eligible seeds inside the search space/Sierpinski triangle, and d is the dimension of these seeds [57]. The seeds' initial positions s_i^j are determined randomly as:

$$s_i^j = x_{i,min}^j + r \cdot (s_{i,max}^j - s_{i,min}^j) \quad (15)$$

where r is a random number within $[0,1]$, and $s_{i,min}^j, s_{i,max}^j$ are the lower boundary (LB) and upper boundary (UB) for the j th decision variable of the i th solution, respectively. The initial seeds generated reflect the primary patterns of dynamic systems based on the theory of chaos. For each of the eligible seeds in the search space (S_i), a temporary position triangle is drawn with three seeds: the defined Global Best (GB), the mean value for each Group (M_{Gi}), and the i th solution applicant (S_i) as the certain seed. The three seeds are positioned in the S_i , GB, and M_{Gi} , respectively. The mathematical presentation of the first seed process is given as:

$$\text{Seed}_i^1 = S_i + x_i * (y_i * GB - z_i * M_{Gi}) \quad (16)$$

where x_i, y_i, z_i represent the random integer of 0 or 1 for modelling the possibility of rolling a dice [58]. Then, the schematic presentation of the described process of the second, third and fourth seeds is formulated as:

$$\text{Seed}_i^2 = GB + x_i * (y_i * S_i - z_i * M_{Gi}) \quad (17)$$

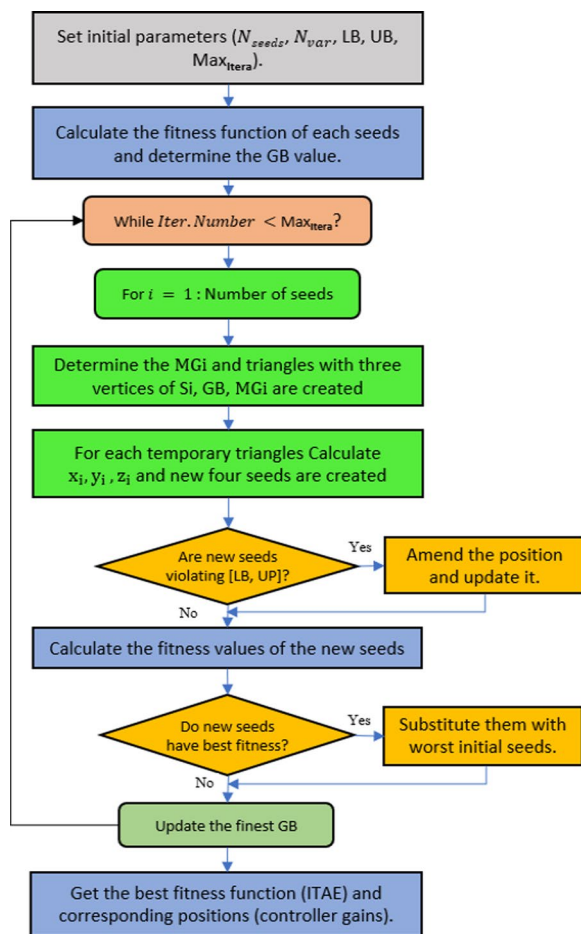
$$\text{Seed}_i^3 = M_{Gi} + x_i * (y_i * S_i - z_i * GB) \quad (18)$$

$$\text{Seed}_i^4 = S_i (s_i^k = s_i^k + r) \quad (19)$$

where k is a random integer within $[1, d]$. To control and adjust the exploitation and exploration rate of the CGO algorithm, four different formulations are presented for x_i which controls the movement boundaries of the seeds [44]:

$$x_i = \begin{cases} r \\ 2 * r \\ \delta * r + 1 \\ \varepsilon * r + \sim \varepsilon \end{cases} \quad (20)$$

where δ and ε are random integers within $[0, 1]$. The flowchart of the CGO algorithm is shown in Fig. 7. The consistency of the new solution candidates is compared

**Fig. 7** Flowchart of CGO

to the previous ones and the lowest value is retained and the seeds with the worst fitness values are excluded equal to the worst degree of self-similarity. When the solution variables (s_i^j) violate the limit conditions, a measured flag is specified in which a boundary change is ordered for s_i^j . The optimization process is terminated after a maximum number of iterations have been completed.

To attain the finest gains of the FOPID–FOPI variables, CGO requires to set the one parameter which is the number of seeds (N_{seeds}), making it a low number of runs required. The CGO algorithm is well-matured and is one of the most likely evolutionary schemes employed to solve complex engineering optimization problems, while the robustness and exploratory capability of the CGO depend on the nature and complexity of the problems.

Table 1 Comparison of ITAE values over 20 independent runs for various schemes (Test-system-1)

Algorithm	Minimum	Maximum	Average	St. deviation
PSO	0.0142	0.0205	0.016051	0.002167
DE	0.0110	0.0183	0.013203	0.002105
CGO	0.0091	0.0139	0.009658	0.001245

5 Results and discussion

The four test systems are investigated to demonstrate the efficacy of the proposed scheme. An FO calculus toolbox for system modeling and control design with 1 ms time step, running on an Intel Core i5 2.1 GHz processor with 8 GB of RAM, is used to simulate the proposed FOPID–FOPI controller in MATLAB/Simulink (2017b). The settling time (T_s) is calculated at 2% of SLP. The CGO procedures and the ITAE criterion are written in .mfile, and the CGO file is linked to the Simulink file for J_{ITAE} calculation. CGO employed for LFC studies is carried out before running the test systems. In each test system, to ascertain the robustness of the proposed strategy, a powerful test is applied that is capable of challenging the proposed CGO: FOPID–FOPI scheme.

5.1 Test-system 1 implementation

5.1.1 Application of CGO to LFC studies

According to the literature, the DE and PSO algorithms are capable of solving LFC issues based on different controller structures, number of areas, and different power plants [11, 59–62]. Thus, initially, to test the suitability of CGO for LFC studies, a comparison with the DE algorithm and PSO based on the proposed FOPID–FOPI controller by taking the error performance function ITAE criterion under 10% SLP at area 1 in Test-system 1 is executed. The dominant parameter of meta-heuristic algorithms is the population size. According to [63], “large initial population sizes do not outperform small populations in terms of identifying the optimum solution”. Therefore, the number of seeds in CGO is set to 15, which is sufficient to obtain an optimum solution and taking up less processing time, and the iteration number is 50 and is performed 20 times to select the best gains of the FOPID–FOPI controller corresponding to the lowest ITAE value. The default MATLAB parameter settings in PSO are used with a population size of 50 [64]. The DE parameters are population size ($NP=50$), the number of

Table 2 Optimized controller parameters and ST and J_{ITAE} results of Test-system-1

Algorithm	ISFS: PID [1]	DSA: FOPID [23]	DSA: FOPI–FOPD [23]	CGO: FOPID–FOPI
Controller parameters	$K_P = 1.6293$ $K_I = 2.0000$ $K_D = 0.5882$	$K_P = 2.0331$ $K_I = 2.9999$ $K_D = 0.4670$ $\lambda = 1.0007$ $\mu = 1.0517$	$K_{P1} = 1.2485$ $K_{P2} = 2.9999$ $K_I = 2.9998$ $K_D = 3.0000$ $\lambda = 1.1007$ $\mu = 0.6312$	$K_{P1} = 3.0000$ $K_{P2} = 0.9700$ $K_{I1} = 2.975$ $K_{I2} = 3.0000$ $K_D = 2.1678$ $\lambda_1 = 0.0298$ $\lambda_2 = 0.9977$ $\mu = 0.9078$
$ST(s)$ (% band)				
ΔF_1	2.15	1.13	0.72	0.46
ΔF_2	3.66	2.73	1.48	1.18
ΔP_{tie12}	3.01	2.23	0.86	0.61
J_{ITAE}	n/a	0.0778	0.0180	0.0091

generations ($G=30$), step size ($F=0.2$), and crossover probability ($CR=0.6$) [65].

The standard deviation, average, maximum, and minimum of ITAE values are displayed in Table 1. From the statistical analysis in Table 1, the minimum value of ITAE is obtained using the proposed CGO algorithm

($ITAE=0.0091$). This compares with DE ($ITAE=0.0110$) and GA ($ITAE=0.0142$). It is concluded that the proposed CGO algorithm is superior to other schemes in terms of average, minimum, and standard deviation values.

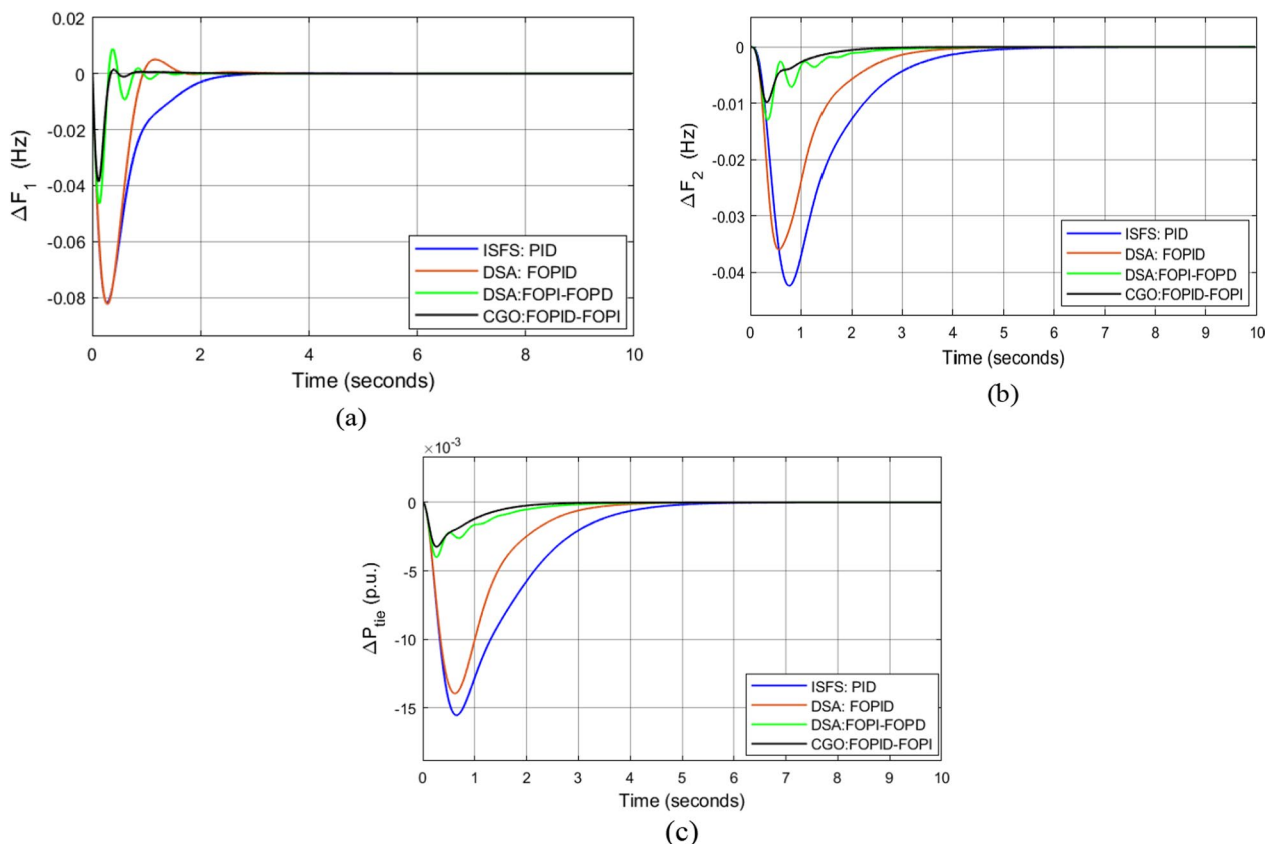


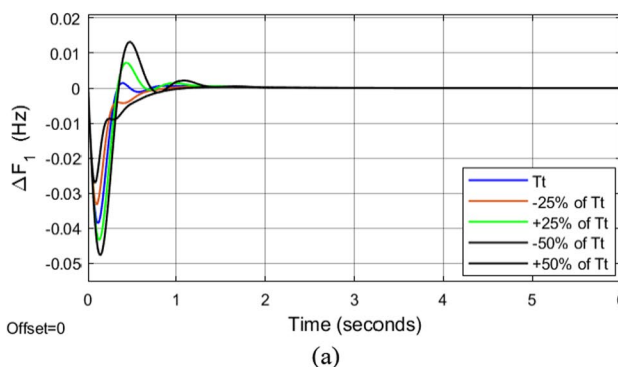
Fig. 8 Comparison of dynamic responses for Test-system 1 under 10% SLP in area 1: **a** ΔF_1 , **b** ΔF_2 , and **c** ΔP_{tie}

5.1.2 Investigation scenarios

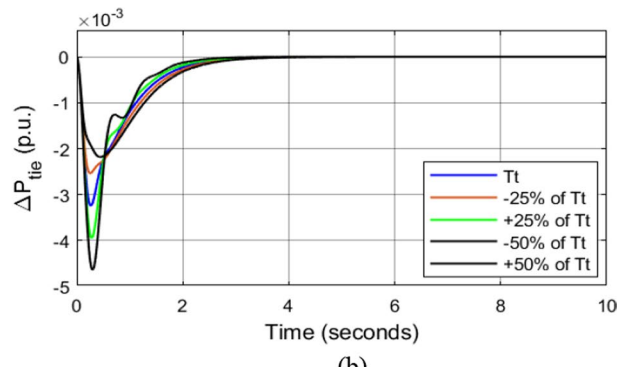
The investigation scenarios are listed below.

1. The proposed CGO: FOPID–FOPI scheme is investigated and compared with other newly published schemes when the first area is exposed to a 10% SLP.

2. Some system parameters increase and decrease by 25% and 50% under $\Delta P_{L1} = 10\%$ SLP to demonstrate the stability of the system.
3. The first and second areas simultaneously undergo a 10% and 20% SLP, respectively, i.e., $\Delta P_{L1} = 10\%$ SLP and $\Delta P_{L2} = 20\%$ SLP.

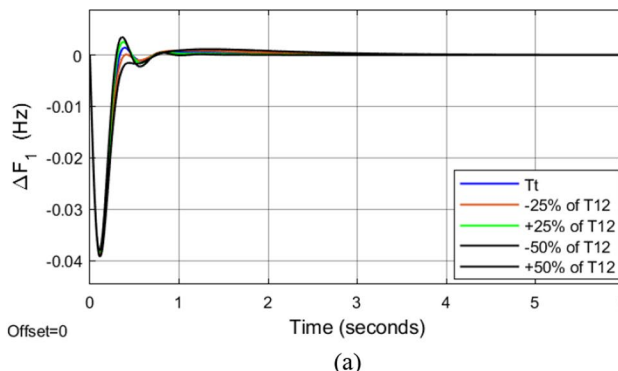


(a)

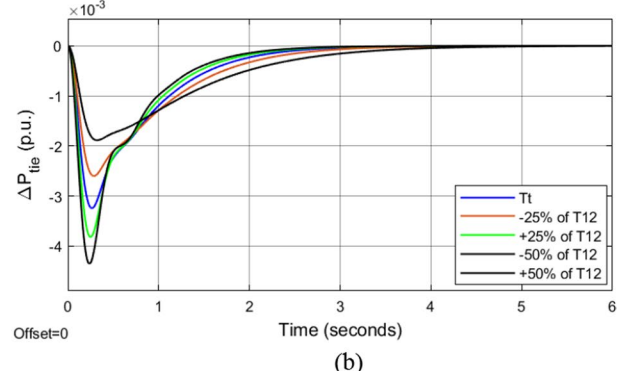


(b)

Fig. 9 Sensitivity analysis under variation of T_t : **a** ΔF_1 and **b** ΔP_{tie}

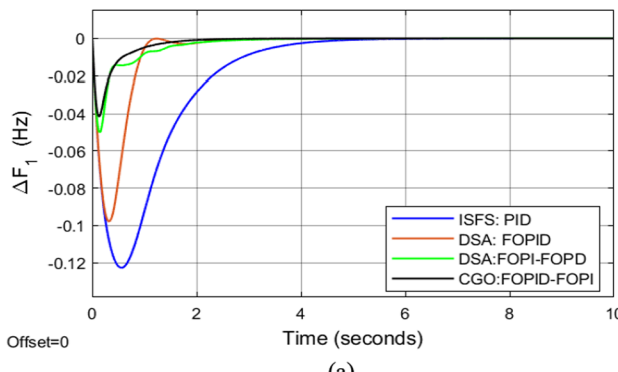


(a)

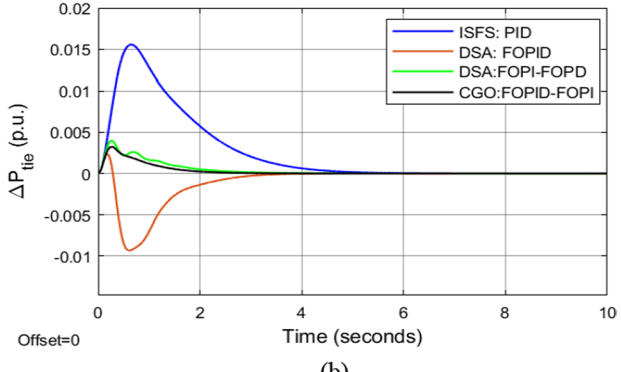


(b)

Fig. 10 Sensitivity analysis under variation of T_{12} : **a** ΔF_1 and **b** ΔP_{tie}



(a)



(b)

Fig. 11 Transient responses under 10% SLP in area 1 and 20% SLP in area 2: **a** ΔF_1 and **b** ΔP_{tie}

For scenario 1, the adjusted controller parameters of CGO: FOPID–FOPI with 10% SLP and the competitors, and the performance analysis of ST and objective function ITAE values for Test-system 1 are presented in Table 2. CGO: FOPID–FOPI has the lowest J (ITAE = 0.0091). This compares with DSA: FOPD–FOPI (ITAE = 0.0180) and DSA: FOPI (ITAE = 0.0778). In addition, the settling times are greatly reduced in both frequency and tie-line power deviations. Figure 8 shows the dynamic response for a 10% SLP in area 1, i.e., Fig. 8a, b show the deviations in frequency in area 1 (Δf_1) and area 2 (Δf_2), respectively, and the tie-line power deviation (ΔP_{tie}) is shown in Fig. 8c. It is seen from Fig. 8 and Table 2 that the proposed method outperforms all rivals in terms of objective function values and settling times, validating the efficacy and robustness of the proposed technique.

In scenario 2, to determine the resilience of the closed-loop system, the power system dynamic behavior is evaluated based on variations in loading circumstances and system parameters. Some system parameters decrease and increase by 25% and 50% under $\Delta P_{L1} = 10\%$ SLP at area 1 to verify system stability. Figures 9 and 10 depict the sensitivity analysis for T_t and T_{12} , respectively. The results indicate that the proposed controller is resilient and works effectively in the event of parameter changes of up to 50%.

In scenario 3, another study of a 10% step load increase in area 1 and a 20% SLP in area 2 is carried out to conclude the investigation of this test system. Figure 11 depicts the transient temporal responses which show that the proposed CGO: FOPID–FOPI performance outperforms the rivals.

5.2 Test-system 2 investigation

The nonlinearity of GDB is examined to assess the superiority of the proposed CGO: FOPID–FOPI, as the instant response of the governor valve to the variation of the input signal is inapplicable. The nonlinearity of GDB creates greater fluctuations and reduces the power system's overall stability [48]. To evaluate the proposed scheme's performance under GDB, a 1% SLP at $t=0$ is applied to the first region. Table 3 shows the tuned gains for the FOPID–FOPI controller, and the resulting cost function (ITAE) is compared with previously documented techniques, such as DSA-based FOPI–FOPD and FOPID controllers [23], and ISFS: PID [1], to illustrate the superiority of the proposed strategy. As seen from Table 3, the best value of ITAE is obtained using the proposed CGO: FOPID–FOPI (ITAE = 0.0028). This compares with DSA: FOPI–FOPD (ITAE = 0.0034) and DSA: FOPI (ITAE = 0.0121) controllers. In addition, the transient responses of the proposed regulators and the other schemes at 1% at area 1 are compared in Fig. 12, while the ST of the system responses Δf_1 , Δf_2 , and ΔP_{tie} are also shown in Table 3. From Table 3 and Fig. 12, it can be seen that using the proposed method, GDB's settling times are improved. The proposed method outperforms the compared schemes in terms of GDB nonlinearity, something which poses a practical obstacle to power systems in operation.

5.3 Test-system 3 investigation

The proposed CGO: FOPID–FOPI CC outperforms others in a more realistic IPS paradigm with six units supplying a given load under varying conditions. In the first

Table 3 Optimized controller parameters and ST and J_{ITAE} results of Test-system-2

Algorithm	ISFS: PID [1]	DSA: FOPID [23]	DSA: FOPI–FOPD [23]	CGO: FOPID–FOPI
Controller parameters	$K_p = 0.3898$ $K_i = 1.0113$ $K_D = 0.7695$	$K_p = 2.5578$ $K_i = 2.9999$ $K_D = 0.7937$ $\lambda = 1.0020$ $\mu = 1.2510$	$K_{P1} = 2.3181$ $K_{P2} = 2.9999$ $K_i = 2.9879$ $K_D = 0.4391$ $\lambda = 1.0000$ $\mu = 1.4642$	$K_{P1} = 2.3126$ $K_{P2} = 1.6944$ $K_i = 2.9913$ $K_D = 2.6311$ $\lambda_1 = 1e-8$ $\lambda_2 = 1.0000$ $\mu = 1.5000$
<i>ST (s) (2% band)</i>				
Δf_1	6.25	2.34	1.22	1.708
Δf_2	6.48	3.63	2.25	1.95
ΔP_{tie}	4.40	2.33	1.05	0.84
J_{ITAE}	n/a	0.0121	0.0034	0.0028

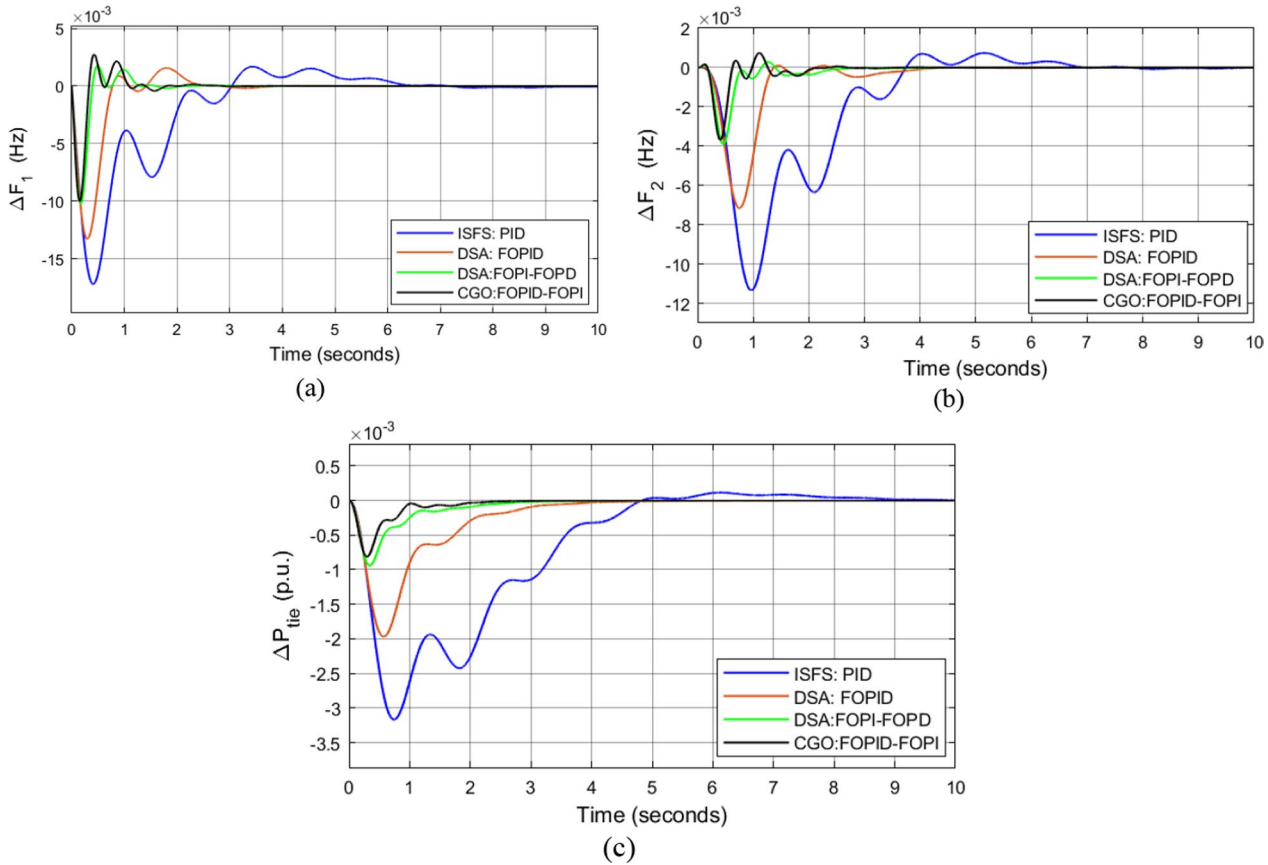


Fig. 12 Comparison of dynamic responses for Test-system 2 under 1% SLP in area 1: **a** ΔF_1 , **b** ΔF_2 , and **c** ΔP_{tie}

area, the controller settings are tuned under 2% SLP. Table 4 shows the improved controller settings as well as some system outcomes obtained with the proposed controller. Compared with other methods such as DSA-based FOPI–FOPD and FOPID controllers [23], and MGWO-based PID controller [27], the CGO: FOVID–FOPI ($ITAE=0.0259$) has the lowest ITAE at 1% load disturbance, demonstrating the applicability of the CGO algorithm for LFC problems in the IPS. This compares with DSA: FOPI–FOPD ($ITAE=0.0461$), DSA: FOVID ($ITAE=1.557$), and MGWO ($ITAE=0.9197$). Table 4 shows the ST from the closed-loop system transient responses, i.e., ΔF_1 , ΔF_2 , and ΔP_{tie} . This demonstrates that the dynamic response in terms of settling times is

considerably improved. Figure 13 depicts the dynamic reaction to a 2% load perturbation in the first area. It is inferred from this scenario that the major characteristics of the dynamic response validate the superiority of the proposed CGO: FOVID–FOPI scheme in a hybrid IPS.

5.4 Test-system 4 investigation

This study extends to a three-area hydrothermal plant and includes the nonlinearity of GRC. When a 1% SLP at $t=0$ is applied in all three areas, the controller variables are adjusted using CGO by minimizing J_{ITAE} . Table 5 summarizes the optimal gains of FOVID–FOPI CC and the associated system results. The results are contrasted with the results of DSA-optimized FOPI–FOPD

Table 4 Optimized controller parameters and ST and J_{ITAE} results of Test-system-3

Algorithm	MGWO: PID [27]	DSA: FOPID [23]	DSA: FOPI–FOPD [23]	CGO: FOPID–FOPI
Controller parameters	<i>Thermal</i> $K_P = 1.7502$ $K_I = -0.0087$ $K_D = 0.7499$ <i>Hydro</i> $K_P = 0.3110$ $K_I = 0.3102$ $K_D = 0.0034$ <i>Gas</i> $K_P = 0.0091$ $K_I = 1.2409$ $K_D = 0.6901$	<i>Thermal</i> $K_P = 1.9998$ $K_I = 2.0000$ $K_D = 1.9999$ $\lambda = 0.5021$ $\mu = 0.2386$ <i>Hydro</i> $K_P = 1.2029$ $K_I = 1.1908$ $K_D = -0.4375$ $\lambda = 0.5072$ $\mu = 0.3748$ <i>Gas</i> $K_P = 0.9272$ $K_I = 2.0000$ $K_D = 1.9999$ $\lambda = 1.2105$ $\mu = 1.2682$	<i>Thermal</i> $K_{P1} = -2.0000$ $K_{P2} = -2.0000$ $K_I = -2.0000$ $K_D = -2.0000$ $\lambda = 0.5040$ $\mu = 0.0100$ <i>Hydro</i> $K_{P1} = 1.7433$ $K_{P2} = -2.0000$ $K_I = -2.0000$ $K_D = -1.3626$ $\lambda = 0.9506$ $\mu = 0.0877$ <i>Gas</i> $K_{P1} = -2.0000$ $K_{P2} = -1.7815$ $K_I = -2.0000$ $K_D = -2.0000$ $\lambda = 0.8692$ $\mu = 1.2000$	<i>Thermal</i> $K_{P1} = 1.9999$ $K_{P2} = 1.9787$ $K_I = 1.9878$ $K_D = 2.0000$ $\lambda_1 = 0.3023$ $\lambda_2 = 0.3013$ $\mu = 1e-9$ <i>Hydro</i> $K_{P1} = 2e-7$ $K_{P2} = 0.1269$ $K_I = 2.1e-8$ $K_D = 1.8441$ $\lambda_1 = 0.0061$ $\lambda_2 = 1.0000$ $\mu = 1.5e-6$ <i>Gas</i> $K_{P1} = 1.5012$ $K_{P2} = 2.0000$ $K_I = 2.0000$ $K_D = 1.6228$ $\lambda_1 = 1.1267$ $\lambda_2 = 1.1e-4$ $\mu = 1.3075$
<i>Ts (s) (2% band)</i>				
ΔF_1	15.69	8.31	1.81	1.74
ΔF_2	20.05	6.25	4.51	3.53
ΔP_{tie}	17.82	6.51	3.98	2.86
J_{ITAE}	0.9197	1.557	0.0461	0.0259

and FOPI–FOPD controllers, as well as ISFS-optimized PID controller, to highlight the capability of the proposed controller.

According to Table 5, CGO: FOPID–FOPI results in a lower value of J_{ITAE} ($ITAE=82.67$) than DSA-adjusted FOPI–FOPD CC ($ITAE=147.56$) and FOPI–FOPI controllers ($ITAE=156.32$), demonstrating that FOPI–FOPI

CC outperforms FOPI–FOPD and FOPI–FOPI controllers in all test systems. Figure 14 shows the transient results of Test-system 4 at 1% SLP in each area. These demonstrate that the proposed method has the lowest undershoot and is the quickest to settle. Thus, the most promising controller is the CGO-optimized FOPI–FOPI CC, which results in significant reduction in settling time

Table 5 Optimized controller parameters, ST and J_{ITAE} results of Test-system-4

Algorithm	ISFS: PID [1]	DSA: FOPID [23]	DSA: FOPI–FOPD [23]	CGO: FOPID–FOPI
Controller parameters	<i>Area 1: Thermal</i> $K_p = 1.1539 * 10^{-12}$ $K_I = 0.0577$ $K_D = 0.1606$ <i>Area 2: Thermal</i> $K_p = 1.1539 * 10^{-12}$ $K_I = 0.0577$ $K_D = 0.1606$ <i>Area 3: Hydro</i> $K_p = 1.1539 * 10^{-12}$ $K_I = 0.0577$ $K_D = 0.1606$	<i>Area 1: Thermal</i> $K_p = 0.0001$ $K_I = 0.1253$ $K_D = 0.1206$ $\lambda = 1.0000$ $\mu = 0.5004$ <i>Area 2: Thermal</i> $K_p = 0.0001$ $K_I = 0.1253$ $K_D = 0.1206$ $\lambda = 1.0000$ $\mu = 0.6354$ <i>Area 3: Hydro</i> $K_p = 0.0001$ $K_I = 0.0264$ $K_D = 0.0350$ $\lambda = 1.0000$ $\mu = 0.7376$	<i>Area 1: Thermal</i> $K_{P1} = 0.0316$ $K_{P2} = 0.3346$ $K_I = 0.3424$ $K_D = 0.0271$ $\lambda = 1.0000$ $\mu = 0.6354$ <i>Area 2: Thermal</i> $K_{P1} = 0.0316$ $K_{P2} = 0.3346$ $K_I = 0.3424$ $K_D = 0.0271$ $\lambda = 1.0000$ $\mu = 0.6354$ <i>Area 3: Hydro</i> $K_{P1} = 0.0316$ $K_{P2} = 0.3346$ $K_I = 0.3424$ $K_D = 0.0271$ $\lambda = 1.0000$ $\mu = 0.6354$	<i>Area 1: Thermal</i> $K_{P1} = 1.9248$ $K_{P2} = 1.4875$ $K_I = 0.3518$ $K_D = 1e-12$ $\lambda_1 = 1.0000$ $\lambda_2 = 0.0930$ $\mu = 1.000$ <i>Area 2: Thermal</i> $K_{P1} = 0.9875$ $K_{P2} = 1.7e-7$ $K_I = 0.2773$ $K_D = 1.3016$ $\lambda_1 = 1.0000$ $\lambda_2 = 1e-5$ $\mu = 1.0000$ <i>Area 3: Hydro</i> $K_{P1} = 0.0020$ $K_{P2} = 0.5422$ $K_I = 0.0305$ $K_D = 0.4657$ $\lambda_1 = 1.0000$ $\lambda_2 = 0.1376$ $\mu = 1.0000$
T_s (s) (2% band)				
ΔF_1	107.6	137.5	90.3	60.59
ΔF_2	107.6	137.5	90.3	60.59
ΔF_3	107.6	137.6	90.0	58.71
ΔP_{tie12}	65.28	109.1	68.7	77.43
ΔP_{tie13}	65.28	109.1	68.7	77.43
ΔP_{tie23}	94.83	130.9	74.7	62.47
J_{ITAE}	n/a	156.32	147.56	82.67

when compared with other methods. Therefore, CGO-optimized FOPID–FOPI CC is proven to be capable of operating successfully in multi-area IPSs with GRC disruption.

6 Conclusions

Using the novel CGO method, optimally adjusted FOPID–FOPI controllers for four test systems using the ITAE objective functions are provided. To test

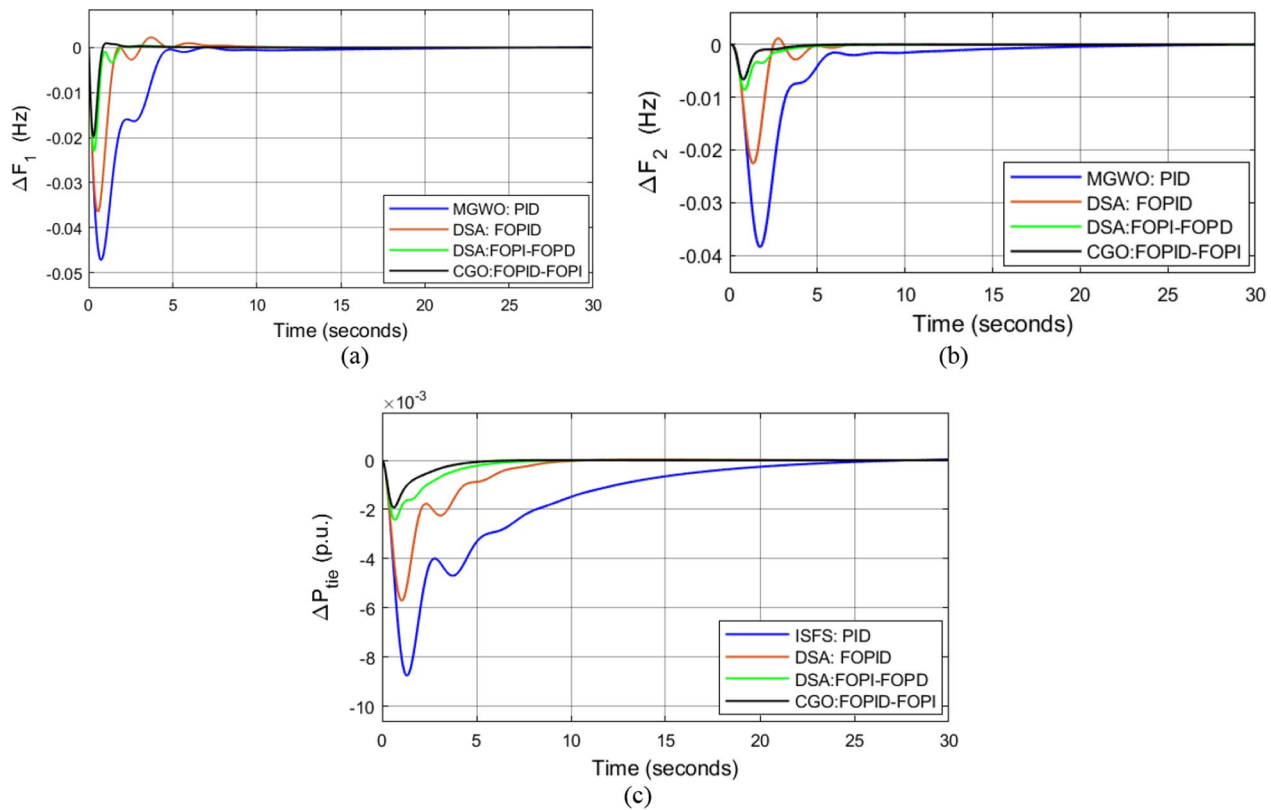


Fig. 13 Comparison of dynamic responses for Test-system 3 under 2% SLP in area 1: **a** ΔF_1 , **b** ΔF_2 , and **c** ΔP_{tie}

and analyze the performance of the CGO: FOPI-FOPI scheme, a typical test system containing a two-area two-unit nonthermal plant with and without GDB nonlinearity is used. To exemplify the proposed approach, a two-area multi-source six-unit test system is investigated. Furthermore, a three-area hydrothermal unit is examined to obtain more realistic results for the LFC study and to illustrate the breadth of application of the proposed FOPI-FOPI CC. The dynamic LFC response patterns of the four test systems investigating IPSs are compared with the results from other recent studies. The dynamic response investigation confirms that FOPI-FOPI outperforms

the conventional PID controller, single-stage FOPID controller, and FOPI-FOPD CC in all trials with lower oscillations and smaller settling time. Finally, the proposed CGO-tuned cascade TD-TI controller is shown to make the LFC framework resilient and produce stable and improved results across a wide range of loading conditions.

In the future, prior to further confirming its robustness, the proposed technique will be evaluated with complicated real-world applications such as LFC with integrated electric vehicles, wind, and PV systems with time delay nonlinearity.

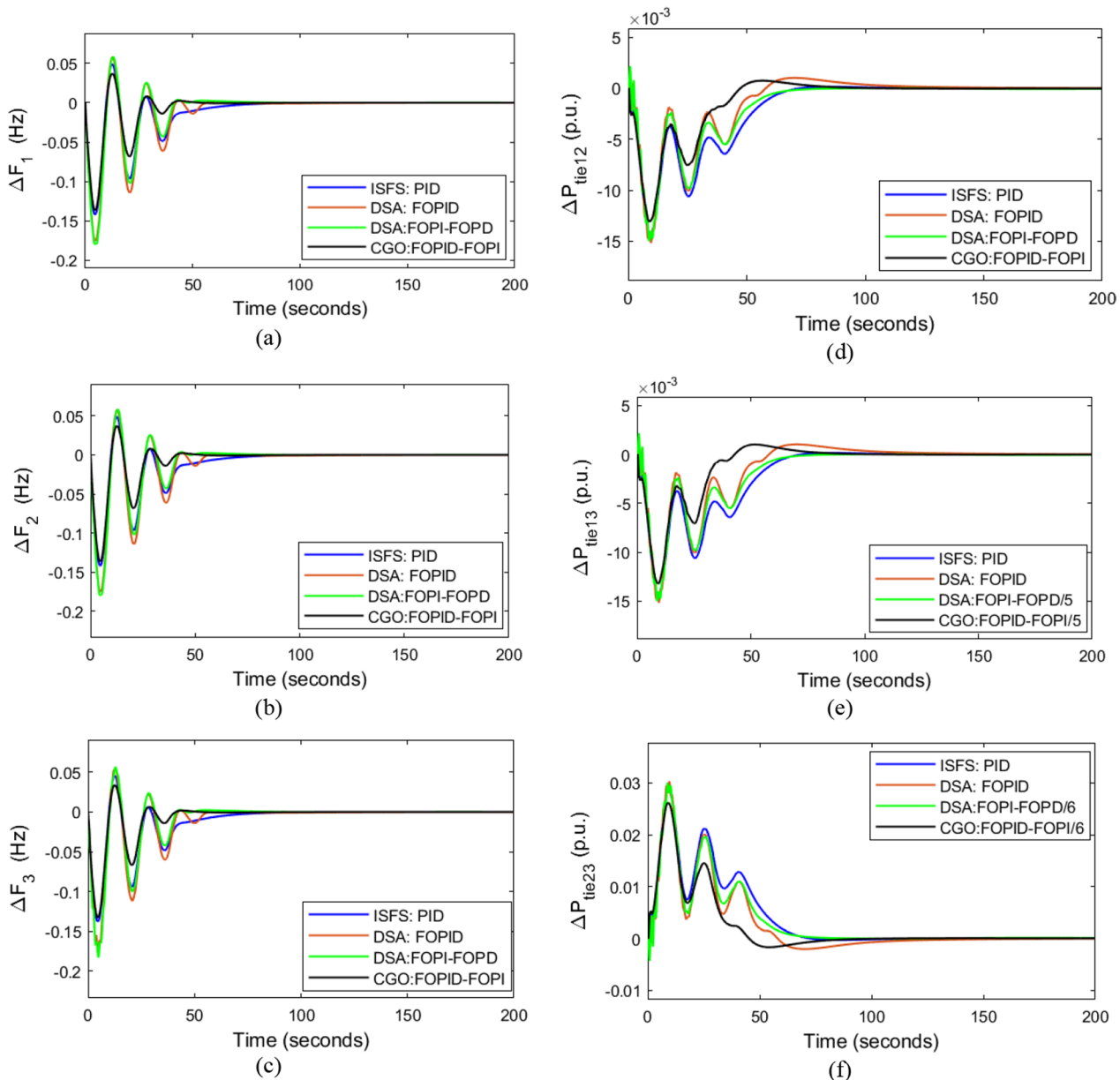


Fig. 14 Comparison of dynamic responses for Test-system 4 under 1% SLP applied in all areas: **a** ΔF_1 , **b** ΔF_2 , **c** ΔF_3 , **d** ΔP_{tie12} , **e** ΔP_{tie13} , and **f** ΔP_{tie23}

Appendix 1: Nominal parameters of two-area two unit (Test-system-1) [23, 59]

$$\begin{aligned} f &= 60 \text{ Hz}; \quad B = 0.425 \text{ p.u MW/Hz}; \quad R = 2.4 \text{ Hz/pu}; \\ T_g &= 0.03 \text{ s}; \quad T_t = 0.3 \text{ s}; \quad K_{PS} = 120 \text{ Hz/pu}; \\ T_{PS} &= 20 \text{ s}; \quad 2 * \pi * T_{12} = 0.545 \text{ p.u MW/rad}. \end{aligned}$$

Appendix 2: Nominal parameters of two-area two unit with GDB (Test-system-2) [23, 59]

$$\begin{aligned} f &= 60 \text{ Hz}; \quad B = 0.425 \text{ p.u MW/Hz}; \quad R = 2.4 \text{ Hz/pu}; \\ T_g &= 0.2 \text{ s}; \quad T_t = 0.3 \text{ s}; \quad K_{PS} = 120 \text{ Hz/pu}; \\ T_{PS} &= 20 \text{ s}; \quad 2 * \pi * T_{12} = 0.444 \text{ p.u MW/rad}. \end{aligned}$$

Appendix 3: Nominal parameters of two-area six unit (Test-system-3) [11, 23]

$$\begin{aligned} P_{rt} &= 2000 \text{ MW}; \quad P_L = 1840 \text{ MW}; \quad B_1 = B_2 = 0.4312 \text{ p.u MW/Hz}; \\ R_1 = R_2 = R_3 &= \frac{2.4 \text{ Hz}}{\text{p.u}}; \quad T_{sg1} = T_{sg2} = 0.08 \text{ s}; \quad T_{t1} = T_{t2} = 0.3 \text{ s}; \\ K_{r1} = K_{r2} &= 0.3; \quad T_{r1} = T_{r2} = 10 \text{ s}; \quad K_{PS1} = K_{PS2} = \frac{68.9566 \text{ Hz}}{\text{p.u}}; \\ T_{PS1} = T_{PS2} &= 11.49 \text{ s}; \quad T_{12} = 0.0433 \text{ p.u.}; \quad \alpha_{12} = -1; \quad T_{w1} = T_{w2} = 1 \text{ s}; \\ T_{RS1} = T_{RS2} &= 5 \text{ s}; \quad T_{RH1} = T_{RH2} = 78.75 \text{ s}; \\ T_{GH1} = T_{GH2} &= 0.2 \text{ s}; \quad X_C = 0.6 \text{ s}; \quad Y_C = 1 \text{ s}; \\ c_g &= 1 \text{ s}; \quad b_g = 0.05 \text{ s}; \quad T_{F1} = T_{F2} = 0.23 \text{ s}; \\ T_{CD1} = T_{CD2} &= 0.2 \text{ s}; \quad T_{CR1} = T_{CR2} = 0.01 \text{ s}; \\ K_T &= 0.543478; \quad K_H = 0.326084; \quad K_G = 0.130438. \end{aligned}$$

Appendix 4 [23]

$$\begin{aligned} f &= 60 \text{ Hz}; \quad B = 0.425 \text{ p.u MW/Hz}; \quad R = 2.4 \text{ Hz/pu}; \quad T_g = 0.08 \text{ s}; \\ T_t &= 0.3 \text{ s}; \quad T_r = 10 \text{ s}; \quad K_r = 0.5 \text{ s}; \quad K_{PS} = 120 \text{ Hz/pu}; \quad T_{PS} = 20 \text{ s}; \\ T_{12} &= T_{12} = T_{12} = 0.086 \text{ p.u MW/rad}; \quad T_W = 1 \text{ s}; \\ K_i &= 5.0; \quad K_d = 4.0; \quad K_P = 1.0; \quad \text{GRC has a saturation } \pm 0.0005. \end{aligned}$$

Abbreviations

IPS: Interconnected power system; LFC: Load frequency control; ACE: Area control error; TF: Transfer function; TS: Time settling; CGO: Chaos game optimization; FO: Fraction-order; PID: Proportional integral derivative; SLP: Step load perturbation; ITAE: Integral time multiplied absolute error; PI: Proportional-integral; TID: Tilt integral derivative; CC: Cascade controller; AGC: Automatic generation control; GDB: And governor dead band; GRC: Generation rate constraint; DC: Direct current; DSA: Dragonfly search algorithm; ISFS: Improved stochastic fractal search.

Acknowledgements

Not applicable.

Author contributions

All authors read and approved the final manuscript.

Funding

The author received no specific funding for this work.

Availability of data and materials

The CGO technique with MATLAB code that helps the findings of this research is offered at <https://link.springer.com/article/10.1007/s10462-020-09867-w>. The FOMCON toolbox, which is used to make FO controllers, is offered at <https://www.mathworks.com/matlabcentral/fileexchange/66323-fomcon-toolbox-for-matlab>. The MATLAB/SIMULINK files can easily be created with the parameter values as demonstrated in the paper.

Declarations

Competing interests

The authors declare that they have no known competing financial interests or personal relationships that could have appeared to influence the work reported in this paper.

Received: 10 September 2021 Accepted: 29 March 2022

Published online: 01 May 2022

References

- Çelik, E. (2020). Improved stochastic fractal search algorithm and modified cost function for automatic generation control of interconnected electric power systems. *Engineering Applications of Artificial Intelligence*, 88, 103407.
- Kundur, P., Balu, N. J., & Lauby, M. G. (1994). *Power system stability and control* (Vol. 7). McGraw-Hill.
- Basler, M. J., & Schaefer, R. C. (2005). Understanding power system stability. In *58th Annual conference for protective relay engineers, 2005* (pp. 46–67).
- Vrdoljak, K., Perić, N., & Šepac, D. (2010). Optimal distribution of load-frequency control signal to hydro power plants. In *2010 IEEE international symposium on industrial electronics* (pp. 286–291).

5. Sahu, R. K., Gorripotu, T. S., & Panda, S. (2015). A hybrid DE-PS algorithm for load frequency control under deregulated power system with UPFC and RFB. *Ain Shams Engineering Journal*, 6(3), 893–911.
6. Tan, W. (2009). Unified tuning of PID load frequency controller for power systems via IMC. *IEEE Transactions on Power Systems*, 25(1), 341–350.
7. Daneshfar, F., Bevrani, H., & Mansoori, F. (2011). Bayesian networks design of load-frequency control based on GA. In *The 2nd international conference on control, instrumentation and automation* (pp. 315–319).
8. Yousef, H. (2015). Adaptive fuzzy logic load frequency control of multi-area power system. *International Journal of Electrical Power & Energy Systems*, 68, 384–395.
9. Talaq, J., & Al-Basri, F. (1999). Adaptive fuzzy gain scheduling for load frequency control. *IEEE Transactions on Power Systems*, 14(1), 145–150.
10. Ali, E. S., & Abd-Elazim, S. M. (2013). BFOA based design of PID controller for two area load frequency control with nonlinearities. *International Journal of Electrical Power & Energy Systems*, 51, 224–231.
11. Mohanty, B., Panda, S., & Hota, P. K. (2014). Controller parameters tuning of differential evolution algorithm and its application to load frequency control of multi-source power system. *International Journal of Electrical Power & Energy Systems*, 54, 77–85.
12. Barisal, A. K. (2015). Comparative performance analysis of teaching learning based optimization for automatic load frequency control of multi-source power systems. *International Journal of Electrical Power & Energy Systems*, 66, 67–77.
13. Sahu, R. K., Panda, S., Rout, U. K., & Sahoo, D. K. (2016). Teaching learning based optimization algorithm for automatic generation control of power system using 2-DOF PID controller. *International Journal of Electrical Power & Energy Systems*, 77, 287–301.
14. Rao, C. S. (2012). Adaptive neuro fuzzy based load frequency control of multi area system under open market scenario. In *IEEE-international conference on advances in engineering, science and management (ICAESM-2012)* (pp. 5–10).
15. Mohamed, T. H., Bevrani, H., Hassan, A. A., & Hiyama, T. (2011). Decentralized model predictive based load frequency control in an interconnected power system. *Energy Conversion and Management*, 52(2), 1208–1214.
16. Liu, X., Kong, X., & Lee, K. Y. (2016). Distributed model predictive control for load frequency control with dynamic fuzzy valve position modelling for hydro-thermal power system. *IET Control Theory and Applications*, 10(14), 1653–1664.
17. Kocaeli, I., & Çam, E. (2005). Fuzzy logic controller in interconnected electrical power systems for load-frequency control. *International Journal of Electrical Power & Energy Systems*, 27(8), 542–549.
18. Sabahi, K., Ghaemi, S., & Pezeshki, S. (2014). Application of type-2 fuzzy logic system for load frequency control using feedback error learning approaches. *Applied Soft Computing*, 21, 1–11.
19. Saikia, L. C., Mishra, S., Sinha, N., & Nanda, J. (2011). Automatic generation control of a multi area hydrothermal system using reinforced learning neural network controller. *International Journal of Electrical Power & Energy Systems*, 33(4), 1101–1108.
20. Yang, B., Zhang, X., Yu, T., Shu, H., & Fang, Z. (2017). Grouped grey wolf optimizer for maximum power point tracking of doubly-fed induction generator based wind turbine. *Energy Conversion and Management*, 133, 427–443.
21. Yang, B., Yu, T., Shu, H., Zhang, X., Qu, K., & Jiang, L. (2018). Democratic joint operations algorithm for optimal power extraction of PMSG based wind energy conversion system. *Energy Conversion and Management*, 159, 312–326.
22. Guha, D., Roy, P. K., & Banerjee, S. (2018). Maiden application of SSA-optimised CC-TID controller for load frequency control of power systems. *IET Generation, Transmission and Distribution*, 13(7), 1110–1120.
23. Çelik, E. (2020). Design of new fractional order PI-fractional order PD cascade controller through dragonfly search algorithm for advanced load frequency control of power systems. *Soft Computing*, 25, 1–25.
24. Franks, R. G., & Worley, C. W. (1956). Quantitative analysis of cascade control. *Industrial and Engineering Chemistry*, 48(6), 1074–1079.
25. Jeng, J.-C., & Liao, S.-J. (2013). A simultaneous tuning method for cascade control systems based on direct use of plant data. *Industrial and Engineering Chemistry Research*, 52(47), 16820–16831.
26. Dash, P., Saikia, L. C., & Sinha, N. (2015). Automatic generation control of multi area thermal system using Bat algorithm optimized PD-PID cascade controller. *International Journal of Electrical Power & Energy Systems*, 68, 364–372. <https://doi.org/10.1016/j.ijepes.2014.12.063>
27. Padhy, S., Panda, S., & Mahapatra, S. (2017). A modified GWO technique based cascade PI-PD controller for AGC of power systems in presence of plug in electric vehicles. *Engineering Science and Technology, an International Journal*, 20(2), 427–442.
28. Guha, D., Roy, P. K., & Banerjee, S. (2018). A maiden application of modified grey wolf algorithm optimized cascade tilt-integral-derivative controller in load frequency control. In *2018 20th National power systems conference (NPSC)* (pp. 1–6).
29. Padhy, S., & Panda, S. (2021). Application of a simplified Grey Wolf optimization technique for adaptive fuzzy PID controller design for frequency regulation of a distributed power generation system. *Protection and Control of Modern Power Systems*, 6(1), 1–16.
30. Morsali, J., Zare, K., & Hagh, M. T. (2017). Applying fractional order PID to design TCSC-based damping controller in coordination with automatic generation control of interconnected multi-source power system. *Engineering Science and Technology, an International Journal*, 20(1), 1–17.
31. Pullaguram, D., Mishra, S., Senroy, N., & Mukherjee, M. (2017). Design and tuning of robust fractional order controller for autonomous microgrid VSC system. *IEEE Transactions on Industry Applications*, 54(1), 91–101.
32. Yang, B., Yu, T., Shu, H., Zhu, D., Zeng, F., Sang, Y., & Jiang, L. (2018). Perturbation observer based fractional-order PID control of photovoltaics inverters for solar energy harvesting via Yin-Yang-Pair optimization. *Energy Conversion and Management*, 171, 170–187.
33. Yang, B., Yu, L., Zhang, X., Wang, J., Shu, H., Li, S., He, T., Yang, L., & Yu, T. (2019). Control of superconducting magnetic energy storage systems in grid-connected microgrids via memetic salp swarm algorithm: An optimal passive fractional-order PID approach. *IET Generation, Transmission & Distribution*, 13(24), 5511–5522.
34. Annamraju, A., & Nadiraju, S. (2019). Robust frequency control in a renewable penetrated power system: An adaptive fractional order-fuzzy approach. *Protection and Control of Modern Power Systems*, 4(1), 1–15.
35. Saxena, S. (2019). Load frequency control strategy via fractional-order controller and reduced-order modeling. *International Journal of Electrical Power & Energy Systems*, 104, 603–614.
36. Morsali, J., Zare, K., & Hagh, M. T. (2018). Comparative performance evaluation of fractional order controllers in LFC of two-area diverse-unit power system with considering GDB and GRC effects. *Journal of Electrical Systems and Information Technology*, 5(3), 708–722.
37. Munagala, V. K., & Jatoh, R. K. (2021). Design of fractional-order PID/PID controller for speed control of DC motor using Harris Hawks optimization. In R. Kumar, V. P. Singh, & A. Mathur (Eds.), *Intelligent algorithms for analysis and control of dynamical systems* (pp. 103–113). Springer.
38. Arya, Y., & Kumar, N. (2017). BFOA-scaled fractional order fuzzy PID controller applied to AGC of multi-area multi-source electric power generating systems. *Swarm and Evolutionary Computation*, 32, 202–218.
39. Sondhi, S., & Hote, Y. V. (2014). Fractional order PID controller for load frequency control. *Energy Conversion and Management*, 85, 343–353.
40. Taher, S. A., Fini, M. H., & Aliabadi, S. F. (2014). Fractional order PID controller design for LFC in electric power systems using imperialist competitive algorithm. *Ain Shams Engineering Journal*, 5(1), 121–135.
41. Mahto, T., Malik, H., & Saad Bin Arif, M. (2018). Load frequency control of a solar-diesel based isolated hybrid power system by fractional order control using partial swarm optimization. *Journal of Intelligent & Fuzzy Systems*, 35(5), 5055–5061.
42. Topno, P. N., & Chanaana, S. (2018). Load frequency control of a two-area multi-source power system using a tilt integral derivative controller. *Journal of Vibration and Control*, 24(1), 110–125.
43. Alhelou, H. H., Hamedani-Golshan, M.-E., Zamani, R., Heydarian-Foroushani, E., & Siano, P. (2018). Challenges and opportunities of load frequency

- control in conventional, modern and future smart power systems: A comprehensive review. *Energies*, 11(10), 2497.
- 44. Talatahari, S., & Azizi, M. (2020). Chaos game optimization: A novel metaheuristic algorithm. *Artificial Intelligence Review*, 54, 1–88.
 - 45. Talatahari, S., & Azizi, M. (2020). Optimization of constrained mathematical and engineering design problems using chaos game optimization. *Computers & Industrial Engineering*, 145, 106560.
 - 46. Ramadan, A., Kamel, S., Hussein, M. M., & Hassan, M. H. (2021). A new application of chaos game optimization algorithm for parameters extraction of three diode photovoltaic model. *IEEE Access*, 9, 51582–51594.
 - 47. Jiang, P., Liu, Z., Wang, J., & Zhang, L. (2021). Decomposition-selection-ensemble forecasting system for energy futures price forecasting based on multi-objective version of chaos game optimization algorithm. *Resources Policy*, 73, 102234.
 - 48. Gheisarnejad, M. (2018). An effective hybrid harmony search and cuckoo optimization algorithm based fuzzy PID controller for load frequency control. *Applied Soft Computing*, 65, 121–138.
 - 49. Barakat, M., Donkol, A., Hamed, H. F. A., & Salama, G. M. (2021). Harris Hawks-based optimization algorithm for automatic LFC of the interconnected power system using PD–PI cascade control. *Journal of Electrical Engineering & Technology*, 16, 1–21.
 - 50. Magdy, G., Mohamed, E. A., Shabib, G., Elbaset, A. A., & Mitani, Y. (2018). SMES based a new PID controller for frequency stability of a real hybrid power system considering high wind power penetration. *IET Renewable Power Generation*, 12(11), 1304–1313.
 - 51. Singhal, R., Padhee, S., & Kaur, G. (2012). Design of fractional order PID controller for speed control of DC motor. *International Journal of Scientific and Research Publications*, 2(6), 1–8.
 - 52. Al-Saggaf, U., Mehedi, I., Bettayeb, M., & Mansouri, R. (2016). Fractional-order controller design for a heat flow process. *Proceedings of the Institution of Mechanical Engineers, Part I: Journal of Systems and Control Engineering*, 230(7), 680–691.
 - 53. Oustaloup, A., Levron, F., Mathieu, B., & Nanot, F. M. (2000). Frequency-band complex noninteger differentiator: Characterization and synthesis. *IEEE Transactions on Circuits and Systems I: Fundamental Theory and Applications*, 47(1), 25–39.
 - 54. Johnson, M. A., & Moradi, M. H. (2005). *PID control*. Springer.
 - 55. Karaboga, D., & Basturk, B. (2007). A powerful and efficient algorithm for numerical function optimization: Artificial bee colony (ABC) algorithm. *Journal of Global Optimization*, 39(3), 459–471.
 - 56. Zaldivar, D., Morales, B., Rodriguez, A., Valdivia-G, A., Cuevas, E., & Perez-Cisneros, M. (2018). A novel bio-inspired optimization model based on Yellow Saddle Goatfish behavior. *Bio Systems*, 174, 1–21.
 - 57. Gao, Z.-M., Zhao, J., Yang, Y., & Tian, X.-J. (2020). The hybrid grey wolf optimization-slime mould algorithm. *Journal of Physics: Conference Series*, 1617(1), 12034.
 - 58. Deepthi, S., & Ravikumar, A. (2015). A study from the perspective of nature-inspired metaheuristic optimization algorithms. *International Journal of Computer Applications*, 113(9), 53–56.
 - 59. Panda, S., Mohanty, B., & Hota, P. K. (2013). Hybrid BFOA–PSO algorithm for automatic generation control of linear and nonlinear interconnected power systems. *Applied Soft Computing*, 13(12), 4718–4730.
 - 60. Veerasamy, V., Wahab, N. I. A., Ramachandran, R., Othman, M. L., Hizam, H., Irudayaraj, A. X. R., Guerrero, J. M., & Kumar, J. S. (2020). A Hankel matrix based reduced order model for stability analysis of hybrid power system using PSO-GSA optimized cascade PI–PD controller for automatic load frequency control. *IEEE Access*, 8, 71422–71446.
 - 61. Safari, A., Babaee, F., & Farrokhiar, M. (2021). A load frequency control using a PSO-based ANN for micro-grids in the presence of electric vehicles. *International Journal of Ambient Energy*, 42(6), 688–700.
 - 62. Mohanty, P., & Sahu, R. K. (2019). Differential evolution optimized cascade tilt-integral–tilt-integral–derivative controller for frequency regulation of interconnected power system. In *International conference on application of robotics in industry using advanced mechanisms* (pp. 104–111).
 - 63. Piotrowski, A. P., Napiorkowski, J. J., & Piotrowska, A. E. (2020). Population size in particle swarm optimization. *Swarm and Evolutionary Computation*, 58, 100718.
 - 64. Barakat, M., Donkol, A., Hamed, H. F. A., & Salama, G. M. (2021). Controller parameters tuning of water cycle algorithm and its application to load frequency control of multi-area power systems using TD-TI cascade control. *Evolving Systems*, 13, 1–16.
 - 65. Sahu, R. K., Panda, S., Biswal, A., & Sekhar, G. T. C. (2016). Design and analysis of tilt integral derivative controller with filter for load frequency control of multi-area interconnected power systems. *ISA Transactions*, 61, 251–264.

Submit your manuscript to a SpringerOpen® journal and benefit from:

- Convenient online submission
- Rigorous peer review
- Open access: articles freely available online
- High visibility within the field
- Retaining the copyright to your article

Submit your next manuscript at ► springeropen.com